RESEARCH ARTICLE
doi: 10.2306/scienceasia1513-1874.2026.066

ScienceAsia 52 (4): 2026: ID 2026066: **1–9**

The enhancement of the efficiency of green hydrogen production through a water separation process using Ni-Cu-doped TiO_2 nanoparticles

Noni Novianti[a], **Fransischa Ramona**[a], **Diana Vanda Wellia**[b], **Mulda Muldarisnur**[a,*]

[a] Department of Physics, Faculty of Mathematics and Natural Sciences, Universitas Andalas, 25163 Indonesia
[b] Department of Chemistry, Faculty of Mathematics and Natural Sciences, Universitas Andalas, 25163 Indonesia

*Corresponding author, e-mail: muldarisnur@sci.unand.ac.id

Received 14 Jan 2026, Accepted 10 Apr 2026
Available online 19 Jul 2026

ABSTRACT: This study aims to investigate the effect of nickel (Ni) and copper (Cu) doping on the efficiency of hydrogen production through water splitting using pure and doped titanium dioxide (TiO_2) photocatalysts. The photocatalysts were synthesized using the sol-gel method, with and without a dopant precursor volume of 1–3 ml. The concentrations of Ni and Cu precursors were varied to investigate their effects on photocatalytic hydrogen evolution. The crystal structure, morphology, particle size, functional groups, and optical properties were characterized using X-ray diffraction, scanning and transmission electron microscopies, Brunauer–Emmett–Teller analysis, Fourier-transform infrared spectroscopy, Raman spectroscopy, and ultraviolet-visible spectroscopy. All samples exhibited a dominant anatase TiO_2 phase, with a main diffraction peak at the (101) plane and nanometer-scale crystallite sizes. The SEM and TEM images revealed an almost spherical particle morphology with a uniform dopant distribution. FTIR spectra confirmed successful doping with the appearance of characteristic metal-oxygen vibration bands (Ni-O, Cu-O, and Ti-O) and an increase in the intensity of surface-OH groups. UV-Vis analysis revealed that Ni and Cu doping reduced the band gap and improved visible-light absorption. The evaluation of photocatalytic activity revealed a significant increase in hydrogen production following doping. The increased hydrogen generation rate with dopant content indicates improved charge separation and electron transfer efficiency. The optimized Ni-Cu co-doped TiO_2 had the highest hydrogen evolution rate compared to pure TiO_2 and the single-metal-doped samples. The synergistic roles of Ni as a proton-reduction site and Cu as a charge-separation promoter improved photocatalytic efficiency.

KEYWORDS: Ni-Cu-doped TiO_2, photocatalyst, water splitting, hydrogen, sol-gel

INTRODUCTION

Global reliance on fossil fuels has resulted in many environmental dilemmas, the most serious of which is global warming. Hydrogen is a promising clean and sustainable energy source. In contrast to fossil fuels, hydrogen is energy-dense, abundant, renewable, and can be produced from various sources [1]. The main problem with hydrogen energy is that most of its production is still based on traditional methods such as steam methane reforming, natural gas decomposition, partial oxidation, and coal gasification [2]. Traditional hydrogen production methods use fossil fuels and emit large amounts of carbon; thus, they are a major driver of climate change and are not environmentally friendly. In addition, these processes are performed at high temperatures, require a lot of energy, and produce hydrogen that is often contaminated and needs to be purified. Carbon capture technology can be added, but the cost will significantly increase.

Producing hydrogen by splitting water using sunlight and photocatalysts is an eco-friendly and sustainable method. It leverages two naturally abundant resources, water and sunlight, and does not emit carbon dioxide [3]. Titanium dioxide (TiO_2) is the most popular photocatalyst due to its stability, non-corrosiveness, low cost, and environmentally friendly nature [4]. Nonetheless, the hydrogen production efficiency from water remains low. This low efficiency is mainly due to the high rate of recombination of electron-hole pairs, the occurrence of fast backward reactions, and the inability of TiO_2 to absorb visible light because of its wide band gap (∼3.2 eV) [5–7].

One approach to address this challenge is to dope TiO_2 nanoparticles with other semiconductors [8], metals [9, 10], or dyes [11]. Doping with noble metals, such as platinum, palladium, and gold, has effectively enhanced photocatalytic efficiency by lowering the electron-hole recombination rate [12]. The plasmonic resonance effect of metals serves as an electron storage [13, 14]. When TiO_2 is exposed to visible light, the resonance excitation of electrons in the conduction band can lead to the generation of high-energy electrons, which can be directly transferred to the TiO_2 conduction band. However, the large-scale use of noble metals is challenging because they are costly and scarce, and thus less economical. Doping TiO_2 with non-noble metals, including chromium (Cr), cobalt (Co), zinc (Zn), iron (Fe), nickel (Ni), and copper (Cu), is a more rational alternative [15]. These metals can reduce the TiO_2 band gap, increase visible-light absorption, inhibit recombination, and improve

catalytic activity.

Photocatalytic water splitting using a TiO_2 photocatalyst with a single dopant (Ni or Cu) was carried out. Ni coating and doping on TiO_2 broaden the visible-light absorption and suppress electron-hole pair recombination, thereby increasing the hydrogen evolution rate [16, 17]. Cu-doping has also been reported to significantly increase hydrogen production by up to several times that of pure TiO_2 [18]. Single-dopant systems are often synthesized under non-identical conditions, making direct performance comparisons difficult. Co-doping strategies that combine two transition metals have attracted attention because of their synergistic effects. Improved charge separation and narrower band gaps in Ni-Fe [19] and Cu-Fe [20] co-doped TiO_2 have been reported to result in higher hydrogen production than that in their mono-doped counterparts. However, few reports exist on Ni-Cu co-doped TiO_2, often relying on complex synthesis methods or lacking systematic comparison with single-doping counterparts [21]. Therefore, comparative studies using a unified synthesis approach are lacking.

Therefore, a thorough analysis of green hydrogen production via photocatalytic water splitting using Ni-Cu co-doped TiO_2 nanoparticles is necessary. This approach directly addresses the major drawbacks of conventional TiO_2 photocatalysts, including poor visible-light absorption, rapid charge recombination, and the need for noble metals. This study is novel because it uses an identical sol-gel protocol to synthesize pure, Ni-doped, Cu-doped, and Ni-Cu co-doped TiO_2. The effects of different dopant concentrations on structural, optical, and photocatalytic properties under identical measurement conditions were systematically compared. Furthermore, we found increased hydrogen evolution resulting from the synergy of the co-dopant, rather than from single-metal modification.

MATERIALS AND METHODS

Synthesis of Ni-Cu doped TiO_2 nanoparticles

Ni-Cu-doped TiO_2 was synthesized using the sol-gel method [22]. In this method, titanium tetraisopropoxide (TTIP, Merck KGaA, Darmstadt, Germany) acts as a TiO_2 precursor. The photocatalyst was prepared by mixing 2.5 ml of deionized water with 10 ml of isopropanol. The obtained solution was stirred for 0.5 h. The required amount of 1 M TTIP was added dropwise to this solution to form a suspension, followed by the addition of 1 ml of HNO_3 to adjust the pH. The solution was stirred vigorously for 45 min. Nickel nitrate hexahydrate and copper nitrate trihydrate were added dropwise to the solution at the desired concentrations with continuous stirring. The obtained gel was dried at 80 °C for 5 h and annealed at 450 °C for 3 h to obtain a doped TiO_2 photocatalyst. The influence of the dopant concentration on the photocatalytic performance was investigated by varying the volumes of nickel and copper nitrates in the precursor solution (1, 2, and 3 ml). The increase in the precursor volume corresponded to increases in the molar percent of the dopant of 1.23%, 2.43%, and 3.61%. This approach enabled the evaluation of the concentration-dependent structural, optical, and photocatalytic behaviors. The selected concentration range was guided by literature reports demonstrating structural stability at transition metal concentrations < 15 mol% [23]. Excessive incorporation may induce defect clustering, which acts as a recombination center. The synthesis process of pure and doped TiO_2 nanoparticles is shown in Fig. 1(a).

Characterization of Ni-Cu doped TiO_2 nanoparticles

The pure and doped TiO_2 nanoparticles were characterized using several instruments. XRD (Bruker D8 Advance, Bruker, Karlsruhe, Germany) was used to determine the crystal structure, crystallinity, and crystallite size of the samples. TEM (Tecnai G2 20S-Twin + EDS, Thermo Fisher Scientific, Massachusetts, USA) and scanning electron microscopy with energy-dispersive X-ray (SEM–EDX; Carl Zeiss EVO 10 with EDX, Carl Zeiss Microscopy GmbH, Germany) were employed to observe the particle shape, lattice constant, surface morphology, and doping distribution. A UV-Vis spectrophotometer (Shimadzu UV-1900i, Shimadzu Corporation, Japan) was used to measure light absorbance. FTIR (Shimadzu FTIR Tracer-100, Shimadzu Corporation, Japan) and Raman Spectroscopy (Bruker Senterra II, Bruker) were used to investigate the chemical bonding between doping and TiO_2 nanoparticles. BET (Anton Paar Nova 800, Anton Paar QuantaTec Inc., Florida, USA) was used to measure the surface area.

Evaluation of photocatalytic activity

The photocatalytic water-splitting performance of the synthesized pure and doped TiO_2 photocatalysts was evaluated using the photoreactor system shown in Fig. 1(b). For each experiment, 80 mg of the photocatalyst powder was dispersed in a 0.5 M Na_2SO_4 aqueous solution. The electrolyte served as an inert reaction medium, enhancing the ionic conductivity without the need for sacrificial agents. The nanoparticles were magnetically stirred continuously to obtain a homogeneous dispersion and prevent particles from settling [24]. A 300 W Xenon lamp (UV-visible range) was placed 20 cm above the suspension surface to irradiate the photoreactor. The reaction system was placed in a closed chamber to minimize the influence of the external light. All samples were illuminated under identical geometric and illumination conditions to confirm a valid comparative analysis. Before illumination, the photocatalyst suspension was stirred in the dark for 30 min to create an adsorption-desorption equilibrium. Dark control experiments were conducted

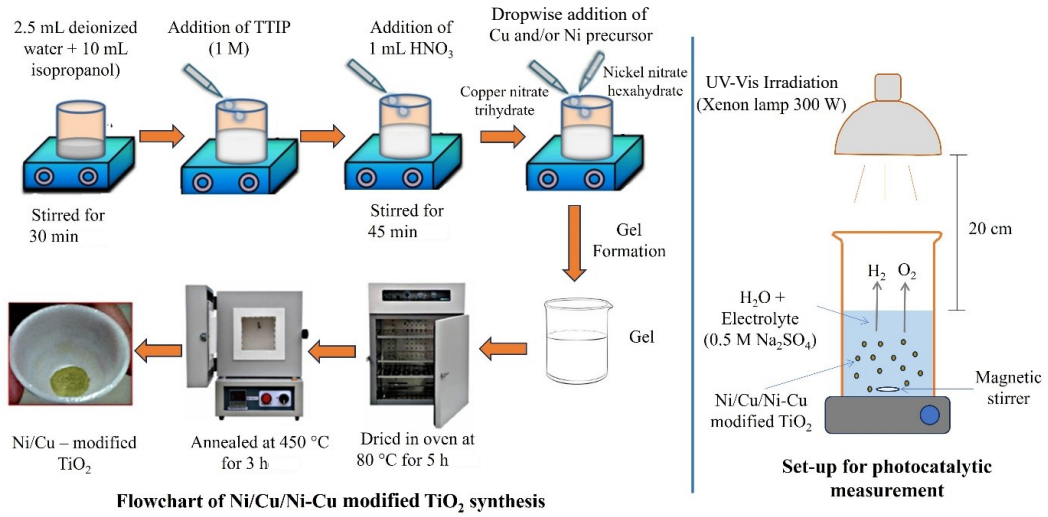

Fig. 1 (a) Flowchart for the synthesis of pure and doped TiO_2 nanoparticles and (b) schematic diagram of photocatalytic water-splitting measurement.

under identical conditions in the absence of light to evaluate non-photocatalytic hydrogen generation. A blank experiment without a photocatalyst was performed under identical irradiation conditions. Gas bubbles were observed on the illuminated surface of the photocatalyst suspension during irradiation. Visual observation and counting of gas bubbles have been used in previous photocatalytic studies to compare relative trends in hydrogen evolution. Although less precise than gas chromatography, bubble counting provides a practical, semi-quantitative method for evaluating comparative activity under identical experimental conditions [17, 25].

The evolution of gas bubbles on the surfaces of the illuminated photocatalysts was visually recorded and counted at fixed irradiation intervals as an indirect method for estimating hydrogen gas evolution. The formation of gas bubbles can be attributed to the photocatalytic water-splitting process, yielding hydrogen and oxygen in a stoichiometric 2:1 mol ratio. The efficiency of the photocatalysts for hydrogen evolution was measured based on the amount of gas bubbles produced under the same time and intensity of illumination. The photocatalytic experiment was repeated three times to confirm the results. The hydrogen production rates are reported as mean ± standard deviation.

RESULTS AND DISCUSSION

XRD analysis

The XRD patterns of pure and doped TiO_2 are shown in Fig. 2. The XRD diffraction patterns revealed that all Ni-doped, Cu-doped, and Ni-Cu co-doped TiO_2 samples exhibited an anatase phase with a tetragonal crystal structure. Anatase is characterized by a prominent (101) peak at approximately $2\theta \approx 25$, which is in good agreement with the ICDD standard data (JCPDS No. 21-1272). The XRD patterns show no detectable secondary phases corresponding to NiO or CuO. Their absence suggests that the dopants were either incorporated into the TiO_2 lattice or highly dispersed below the detection limit. A slight shoulder-like feature in the 35–40° region was attributed to peak broadening and lattice distortion caused by dopant incorporation instead of the formation of a secondary phase. The crystallite sizes of each sample were 3.61 nm (Ni-doped TiO_2), 5.02 nm (Cu-doped TiO_2), and 3.57 nm (Ni-Cu co-doped TiO_2), with the crystallinity degrees

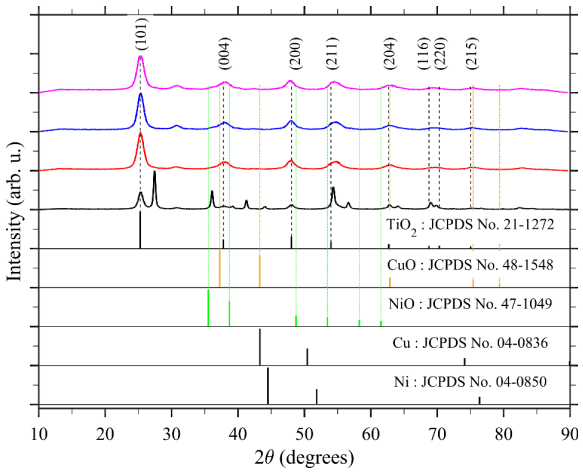

Fig. 2 XRD diffractogram of undoped TiO_2, Ni-doped TiO_2, Cu-doped TiO_2, and Ni-Cu co-doped TiO_2. Standard diffraction peaks for pure TiO_2, Ni, Cu, NiO, and CuO are also shown in the figure.

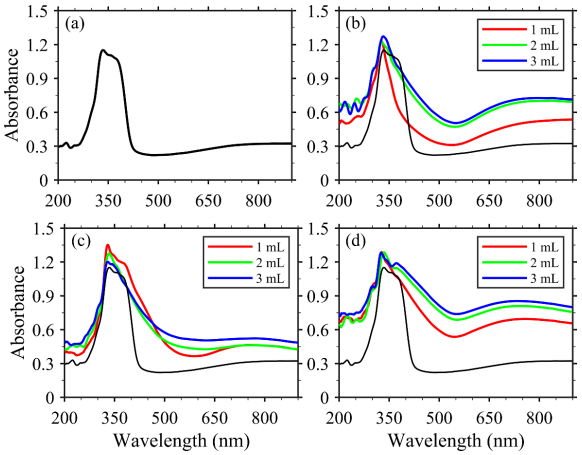

Fig. 3 UV-Vis absorbance spectra of (a) TiO_2, (b) Ni-doped TiO_2, (c) Cu-doped TiO_2, and (d) Ni-Cu co-doped TiO_2 nanoparticles.

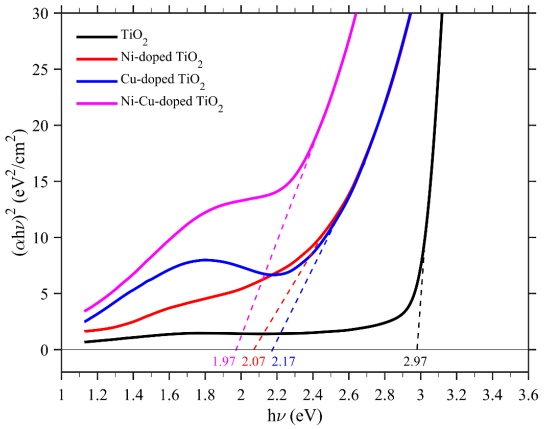

Fig. 4 Band gap energies of undoped TiO_2 and Ni-, Cu-, and Ni-Cu-doped TiO_2, at a dopant concentration of 3 ml.

of 71.62%, 66.42%, and 60.43%, respectively. The obtained crystal size was smaller than that reported in some published studies for Ni- and Cu-doped TiO_2 [26–28]. Small crystallites indicate that dopants may block crystal growth during calcination through lattice distortion and defect formation. The lack of any notable Ni or Cu peaks reveals that the dopants were probably uniformly spread throughout the TiO_2 lattice as well as the amorphous phase.

The inclusion of Ni^{2+} and Cu^{2+} ions in the TiO_2 lattice changed the distance between the crystal planes (d-spacing), as evidenced by the change in the diffraction peak position compared to that of pure TiO_2. This structural perturbation may result from dopant-induced lattice strain or defect formation, thereby affecting the electronic properties of the material and increasing its photocatalytic activity. Nevertheless, to provide conclusive proof of dopant substitution and oxidation states, surface-sensitive techniques, such as X-ray photoelectron spectroscopy (XPS), must be employed, which are beyond the scope of this study.

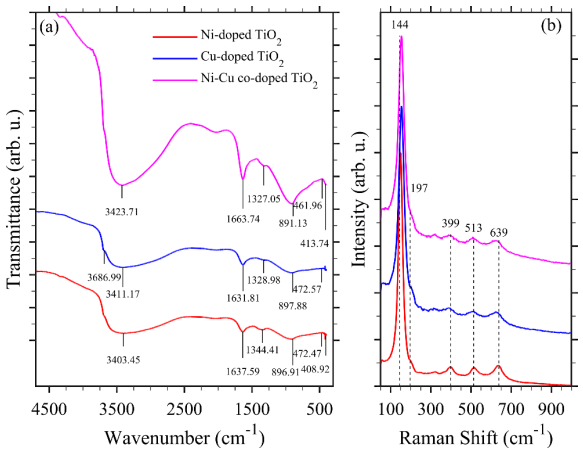

Fig. 5 FTIR spectra of Ni-doped TiO_2, Cu-doped TiO_2, and Ni-Cu co-doped TiO_2 nanoparticles. Spectra were shifted vertically for better comparison.

Ultraviolet-visible spectroscopy (UV-Vis) analysis

A UV-Vis spectrophotometer was used to characterize the optical properties of TiO_2 nanoparticles and Ni-Cu co-doped TiO_2. Fig. 3 presents the absorbance spectra of the samples. Based on the UV-Vis spectrum, pure TiO_2 absorbs strongly only in the ultraviolet region (350–380 nm), which is characteristic of the anatase phase. The absorption increased with doping concentration. Ni doping shifted the absorption edge towards longer wavelengths, indicating the formation of impurity energy levels that reduced the band gap. In Cu-doped TiO_2, the absorption shifts to the visible region (400–700 nm) are more significant due to the role of Cu^{2+} as an electron acceptor. Besides, the formation of oxygen defects acts as additional absorption centers. Ni-Cu co-doping exhibited the most significant synergistic effect, as evidenced by the broadest visible-light absorption and the highest absorbance intensity. Intense visible-light absorption indicates a narrowing of the band gap and an increase in the photon absorption efficiency. An increase in visible-light absorption has the potential to enhance electron–hole pair separation and suppress charge recombination, thereby improving the photocatalytic performance.

The UV-Vis spectra were used to determine the band gap of pure and doped TiO_2 using the Tauc Plot method (Fig. 4). The band gaps of pure, Ni-doped, Cu-doped, and Ni-Cu co-doped TiO_2 were 2.97, 2.07, 2.17, and 1.97 eV, respectively. The band gap of the doped TiO_2 obtained in this study is much smaller than that reported in many literature reports, which are $>$ 2.8 eV.

Vibrational and surface chemical analysis

Doping TiO_2 with copper and nickel could likely cause notable differences in the FTIR spectroscopic fingerprint, indicating modifications in the local atomic bonding and surface properties as a photocatalyst. FTIR analysis is an important method for identifying functional groups and chemical compounds in a sample based on its infrared spectrum. In the case of pure TiO_2, the principal peaks occur in the low wavenumber region (400–700 cm^{-1}) in accordance with the stretching and bending of the Ti-O-Ti bonds. Bands in the region of 3200–3600 cm^{-1} and a peak at 1630 cm^{-1} can be assigned to hydroxyl groups on the surface and adsorbed water. The FTIR spectra are shown in Fig. 5(a). The presence of Cu or Ni in TiO_2 might shift or broaden the Ti-O-Ti bonds, which is associated with lattice distortions caused by introducing Cu^{2+} or Ni^{2+} ions in place of Ti^{4+}, which exhibit size and charge differences. These distortions often cause Ti-O-Cu or Ti-O-Ni bonds. The FTIR spectra exhibited distinct absorption patterns for the Ni-, Cu-, and Ni-Cu-doped TiO_2 samples, indicating successful doping and alterations in the surface chemical structure of TiO_2. Metal ions increase the abundance of surface defects, which exhibit higher hydroxyl group concentrations.

Higher hydroxyl groups are always preferred in photocatalytic water splitting because they serve as sites for oxidation reactions on the TiO_2 surface. Absorption bands at 3400–3600 cm^{-1} corresponding to —OH groups and adsorbed water were observed in all samples, with the most pronounced band broadening in Ni-Cu-doped TiO_2, indicating an increase in the number of —OH groups and water adsorption capacity. The band at 1630 cm^{-1} indicates the bending vibration of bound H_2O molecules. Characteristic bands of Ti-O, Ni-O, and Cu-O bonds appear in the 400–900 cm^{-1} region, validating the interaction of the dopant with the TiO_2 lattice. The Ni-Cu-doped TiO_2 spectrum displayed wider and overlapping bands, demonstrating enhanced lattice distortion due to double doping. Overall, the FTIR results indicate that Ni-Cu-doped TiO_2 underwent the most significant modification of its surface structure, which has the potential to enhance its photocatalytic activity.

The Raman spectra (Fig. 5b) of TiO_2 doped with Ni, Cu, and Ni-Cu show the characteristic vibrational bands corresponding to the anatase TiO_2 host. All bands appear at the same Raman shift, that is, 144 cm^{-1} (symmetric O-Ti-O bending), 197 cm^{-1} (lattice vibration), 399 cm^{-1} (O-Ti-O bending), 513 cm^{-1} (Ti-O stretching), and 639 cm^{-1} (Ti-O stretching). The presence of all bands confirmed the structural integrity of the anatase phase in the doped samples. However, a clear blue shift was observed in the position of the symmetric O-Ti-O bending band of Ni-doped (145 cm^{-1}), Cu-doped (148 cm^{-1}), and Ni-Cu co-doped TiO_2 (∼149 cm^{-1}). The shift in the position of the symmetric O-Ti-O bending band can be attributed to distortion of the crystal lattice resulting from substitutional doping of the TiO_2 lattice with Ni^{2+} and Cu^{2+} ions in place of Ti^{4+} ions.

The characteristic Raman bands for crystalline NiO (∼500–560 and ∼1100 cm^{-1}) and CuO (∼298, 346, and 632 cm^{-1}) were not clearly identified. However, the significant broadening of the high-frequency mode observed at ∼639 cm^{-1} may suggest the presence of defects or highly dispersed NiO/CuO that are not detectable by Raman. The Cu-O vibration mode (∼632 cm^{-1}) may overlap with the anatase E_g mode (∼639 cm^{-1}), resulting in the broadening of the E_g peak instead of the splitting expected when both anatase and CuO are present. The Raman spectroscopy results strongly suggest successful doping of the anatase lattice. The complete exclusion of a small amount of nanocrystalline or highly dispersed copper oxide requires confirmation with more advanced measurements such as XPS.

Secondary phases were not detected in the XRD patterns, and the anatase Raman modes were still present after doping, which together imply that Ni and Cu atoms were successfully incorporated into the TiO_2 lattice at the dopant concentration range studied. Although XPS characterization would offer the most direct and unequivocal evidence for the dopant oxidation states and the surface chemical environment, the predisposition of the instrument prevented it from being performed within the allotted time.

Structural analysis

The SEM–EDX findings are depicted in Fig. 6. The SEM images revealed differences in the surface morphologies of pure and doped TiO_2, which affected their photocatalytic performance. TiO_2 showed a morphology of highly agglomerated nanoparticles with a rough and porous surface texture. The observed morphology was consistent with the small nanoscale crystallite sizes determined by XRD analysis. The Cu-doped TiO_2 particles exhibited a more uniform distribution and a smoother surface. The Ni-Cu-doped TiO_2 specimen exhibited the most uniform morphology with less agglomeration and a larger active surface area. Therefore, the number of available active sites increased, facilitating more efficient electron transfer.

The surface areas of pure TiO_2, Ni-doped, Cu-doped, and Ni-Cu co-doped TiO_2 were 40.4 m^2/g, 119.3 m^2/g, 119.1 m^2/g, and 130.5 m^2/g, respectively. The greater specific surface area of Ni and Cu co-doped TiO_2 in comparison with pure TiO_2 implies that co-doping is effective in preventing the agglomeration of particles, thereby revealing a homogeneous distribution of pores in the structures. An increased surface area provides more accessible active sites, thereby enhancing hydrogen evolution efficiency. The reduction in crystallite size and low crystallinity may lead to an

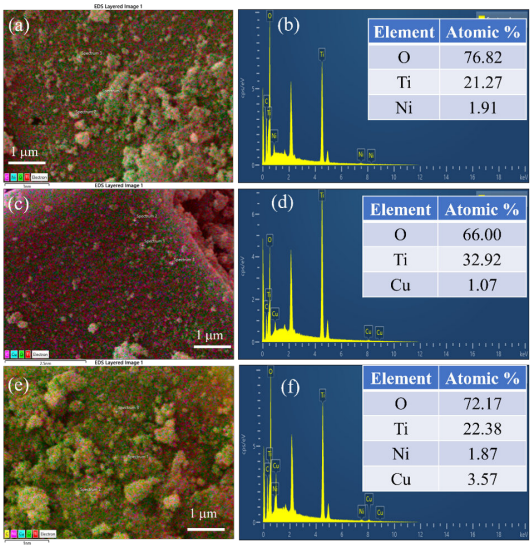

Fig. 6 (a) EDX mapping of Ni-doped TiO_2, (b) elemental atomic percentages of Ni-doped TiO_2, (c) EDX mapping of Cu-doped TiO_2, (d) elemental atomic percentages of Cu-doped TiO_2, (e) EDX mapping of Ni-Cu co-doped TiO_2, and (f) elemental atomic percentages of Ni-Cu co-doped TiO_2 nanoparticles.

increase in the number of defects and surface-active sites, making charge separation easier and enhancing photocatalytic hydrogen evolution. The excellent catalytic activity of the Ni-Cu co-doped TiO_2 sample is mainly due to the structural transformation and an elevated specific surface area, as verified by the BET technique. In addition, the elemental maps obtained from EDX revealed a great mixture of Ti, O, Ni, and Cu in the entire sample, and elemental segregation was not observed. The lack of local Ni- or Cu-rich areas suggests that the dopants were uniformly distributed in the TiO_2 crystal structure and did not exist as separate secondary phases.

TEM was used to characterize morphology and microstructural features. The TEM examination of the Ni- and Cu-co-doped TiO_2 sample, which demonstrated the greatest photocatalytic efficiency, has been discussed. Fig. 7 presents TEM imaging results. High-resolution TEM (HRTEM) images demonstrated that the Ni- and Cu-co-doped TiO_2 particles were < 10 nm in size and had spherical to irregular shapes; no large separate particles were observed. The particles seemed to be closely packed because of their high surface energy. Distinct primary particle features were identified, suggesting that the material consisted of discrete nanoscale domains rather than large bulk aggregates. The detected particle sizes agreed with the average crystallite size estimated from the XRD patterns using the Scherrer equation. This result implies that a single particle is primarily a single-crystalline domain.

Fig. 7b exposes well-defined lattice fringes, indicating the high crystallinity of the sample. The measured interplanar spacing (d-spacing) was approximately 0.35–0.36 nm, matching the (101) plane of the anatase TiO_2 phase. This finding is consistent with the dominant anatase diffraction peak detected in the XRD and Raman analyses. The absence of secondary crystalline phases corroborates the XRD results, which did not show additional diffraction peaks related to NiO, CuO, or metallic Ni/Cu. These findings suggest that Ni and Cu ions were successfully incorporated into the TiO_2 lattice, most likely through substitutional doping. The TEM data confirmed the formation of highly crystalline, single-phase anatase nanocrystallites with sizes < 10 nm.

Photocatalytic activity test

Photocatalytic activity tests were conducted to evaluate the ability of pure, Ni-doped, Cu-doped, and Ni-Cu co-doped TiO_2 to produce hydrogen via photocatalytic water-splitting reactions. The parameter observed in this test was the number of hydrogen bubbles formed as a function of irradiation time (Fig. 8). In the water-splitting reaction experiment, the presence of gas bubbles upon light exposure to the sample confirmed hydrogen production. Bubble formation was not observed in the absence of light (dark control experiment) and without photocatalysts (blank experiment), confirming that hydrogen production originated solely from the photocatalytic activity of the synthesized materials under irradiation.

The steady increase in the number of bubbles with increasing light exposure time confirmed the steady-state nature of the hydrogen evolution reaction in the system. This linear relationship implies a constant rate of photoexcitation, charge separation, and surface redox reactions. The rate at which the number of bubbles increased with exposure time was a measure of the hydrogen evolution rate and photocatalyst efficiency [27]. The steeper the graph of the number of bubbles with light exposure time, the greater the rate of hydrogen evolution and the efficiency of the photocatalyst. Pure TiO_2 exhibited the lowest activity owing to its low light absorption and high electron-hole pair recombination.

Hydrogen evolution was assessed by determining the linear slope of the generated bubbles, as well as the standard deviation and relative standard deviation (RSD). The slope of the undoped TiO_2 was 0.1858 ± 0.0026, with an RSD of 1.40%. As the doping concentration increased with Ni-doped TiO_2, it rose steadily to 0.1929 ± 0.0016 (1 ml, RSD 0.83%), 0.2731 ± 0.0017 (2 ml, RSD 0.64%), and 0.4683 ± 0.0010 (3 ml, RSD 0.21%). The slope for Cu-doped TiO_2 increased to 0.1874 ± 0.0026 (1 ml, RSD 1.40%), 0.2711 ± 0.0038 (2 ml, RSD 1.42%), and 0.3840 ± 0.0055 (3 ml, RSD 1.42%). Ni-Cu co-doped TiO_2 exhibited the highest activity, which increased to 0.4711 ± 0.0051 (1 ml, RSD 1.07%), 0.5901 ± 0.0061

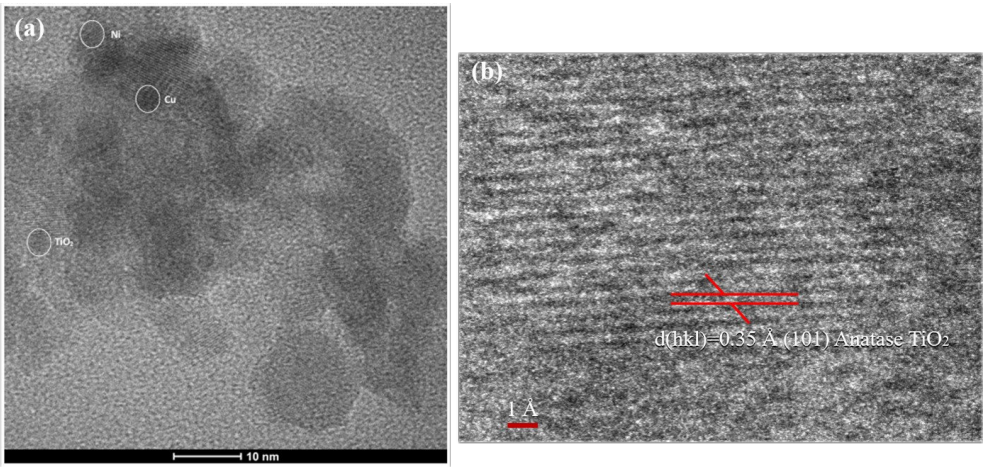

Fig. 7 (a) TEM image showing nanoscale crystallites of Ni-Cu co-doped TiO_2. (b) HRTEM image showing clear lattice fringes. The measured interplanar spacing of ∼0.35 nm corresponds to the (101) plane of anatase TiO_2.

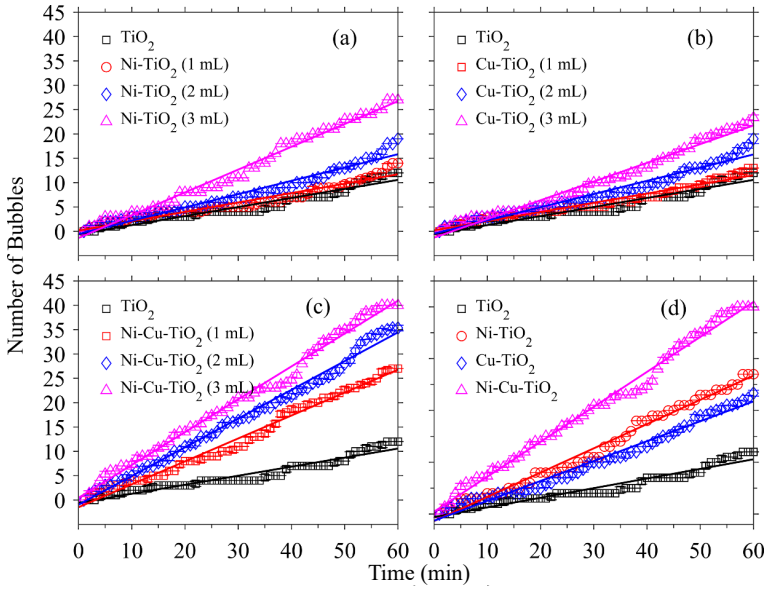

Fig. 8 Photocatalytic activity of TiO_2 and Ni-doped, Cu-doped, and Ni-Cu co-doped TiO_2. (a) Ni-doped TiO_2, (b) Cu-doped TiO_2, (c) Ni-Cu co-doped TiO_2, and (d) comparison of all samples at a dopant concentration of 3 ml.

(2 ml, RSD 1.04%), and 0.6750 ± 0.0040 (3 ml, RSD 0.60%). RSDs of < 1.50% represent good experimental reproducibility. A concentration-dependent enhancement was observed for all doped systems, with Ni-Cu co-doped TiO_2 displaying the most significant improvement. Although differences in reactor configuration and hydrogen quantification methods limit direct comparisons, the observed relative enhancement trend is consistent with previous reports on bimetallic-doped TiO_2 systems. The synergistic effects in this system improve the charge-separation efficiency while increasing the number of accessible active sites. This argument aligns with the increased specific surface area observed in the BET analysis and the enhanced optical absorption behavior.

This result is consistent with previous research, which reported an increased H2 evolution rate when TiO_2 nanoparticles were doped with noble [27] and non-noble [29] metals. These results agree with SEM characterization, which revealed that the morphology of Ni-Cu-doped TiO_2 was more homogeneous and exhibited a larger active surface area. Instead of forming separate NiO or CuO phases, the Ni and Cu species were integrated into the TiO_2 lattice or existed in highly dispersed states. Therefore, lattice doping effects, such as band gap modulation, defect generation, and improved charge-carrier separation, are responsible for the increased photocatalytic activ-

ity. The increased activity found in Ni- and Cu-doped TiO_2 implies that metal incorporation affects charge-transfer behavior. According to earlier research, Ni species can act as electron-trapping or co-catalytic sites that facilitate proton reduction [30, 31]. However, Cu species can accept electrons, thereby suppressing charge recombination [32]. The improved hydrogen evolution rates, along with the increased surface area and modified optical absorption behavior, suggest that the introduction of dopants probably improves the charge-separation efficiency. However, direct charge-carrier dynamics were not examined in this study using photoluminescence or electrochemical measurements.

Depending on the dopants and preparation techniques, numerous hydrogen evolution rates have been reported in recent studies on doped TiO_2 photocatalysts. Ni-doped TiO_2 prepared using wet impregnation achieved hydrogen evolution rates of ∼10.82 mmol/h/g, whereas Ru-loaded samples reached ∼23.9 mmol/h/g under similar irradiation conditions using sacrificial methanol solutions [33]. Additionally, modified hydrothermal Ni-TiO_2 systems exhibited a more moderate enhancement (∼7.32 mmol/h/g) [34]. Visible-light-responsive co-doped systems, such as Cu: Zr–TiO_2, exhibited a rate of ∼1.24 mmol/h/g under visible-light irradiation [35]. In this study, the bubble diameter was approximately 1 mm and remained visually constant throughout the experiment or among different samples. A nearly constant bubble size indicates consistent gas evolution conditions during the measurement. A rough estimation of the hydrogen evolution rate at the highest activity (40 bubbles/min) corresponds to approximately 640 µmol/g/h. This value is lower than that reported in most studies on optimized samples; however, it is still higher than that of similar co-doping (178–198 µmol/g/h) [21] and still shows a meaningful enhancement relative to pure TiO_2. The typical baseline performance of undoped TiO_2 frequently ranges from a few tens to hundreds of µmol/g/h. The relative improvement trend (Ni < Cu < Ni-Cu) observed in this study is consistent with the established performance trends for transition-metal-doped TiO_2 photocatalysts.

According to optical and structural characterizations, the enhancement of the photocatalytic hydrogen evolution activity of Ni-Cu-doped TiO_2 was mainly due to the lattice, doping, and induced optimized electronic structure of TiO_2. XRD and HRTEM studies ruled out the presence of separate NiO, CuO, or metallic phases; thus, Ni^{2+} and Cu^{2+} should be naturally incorporated into the TiO_2 lattice. These substitutions result in lattice distortion and oxygen vacancies, leading to the formation of localized impurity energy levels in the band gap. Defects in these states can lead to an increased absorption of light. They also seem to be able to temporarily trap photogenerated charge carriers, which implies that these trapping sites help to reduce the rapid recombination of electron-hole pairs. Upon light irradiation, electrons in the valence band of TiO_2 are excited to the conduction band, leaving holes. Dopants, by creating defect states, help separate charges by trapping electrons, thus extending their lifetimes and resulting in more electrons available for surface redox reactions. BET analysis revealed an increase in specific surface area, thereby making more active sites accessible for proton reduction. The Ni-Cu-doped TiO_2 catalyst achieved a remarkable hydrogen evolution rate through its efficient light absorption, charge separation, and surface-active sites.

CONCLUSION

In this work, Ni- or Cu-doped TiO_2 nanoparticles were produced. XRD, SEM, TEM, and UV-Vis analyses revealed that the material predominantly consisted of the anatase phase with nanometer-sized crystallites, exhibited an almost spherical shape, and possessed a well-ordered crystalline structure, as confirmed by the d(hkl) value of 0.36 nm on the (101) plane. Ni and Cu doping did not alter the TiO_2 crystalline phase; however, it lowered the band gap, thereby increasing visible-light absorption and ultimately leading to higher photocatalytic activity. The Ni-Cu-doped TiO_2 system showed the highest photocatalytic activity, with a hydrogen generation rate of 3.6 times that of pure TiO_2, even exceeding the rates of Ni-doped TiO_2 and Cu-doped TiO_2. This result confirmed the synergistic effect of Ni-Cu on the enhancement of the water-splitting reaction.

Acknowledgements: This work was supported by Andalas University in accordance with the Research Contract for Master's Thesis Research Scheme, Batch I, Number: 166/UN16.19/PT.01.03/PTM/2025 Fiscal Year 2025.

REFERENCES

1. Rafique M, Hajra S, Irshad M, Usman M, Imran M, Assiri MA, Ashraf WM (2023) Hydrogen production using TiO_2-based photocatalysts: A comprehensive review. *ACS Omega* **8**, 25640–25648.
2. Kumar R, Kumar A, Pal A (2021) An overview of conventional and non-conventional hydrogen production methods. *Mater Today* **46**, 5353–5359.
3. Pareek A, Dom R, Gupta J, Chandran J, Adepu V, Borse PH (2020) Insights into renewable hydrogen energy: Recent advances and prospects. *Mater Sci Energy Technol* **3**, 319–327.
4. Lin B-L, Chen R, Zhu M-L, She A-S, Chen W, Niu B-T, Chen Y-X, Lin X-M (2024) Enhanced photoelectrochemical water splitting performance of Ce-doped TiO_2 nanorod array photoanodes for efficient hydrogen production. *Catalysts* **14**, 639.
5. Kang X, Liu S, Dai Z, He Y, Song X, Tan Z (2019) Titanium dioxide: From engineering to applications. *Catalysts* **9**, 191.
6. Wellia DV, Syafawi A, Putri YE, Muldarisnur M (2023) The effect of cetyltrimethylammonium bromide (CTAB) addition on green synthesis of porous N-doped TiO_2 for

photoreduction of heavy metal ion Cr (vi). *RSC Adv* **13**, 29645–29656.
7. Nantaouppakan W, Comsup N (2025) Effects of calcination heating rate on the photocatalytic activity of Al-doped TiO_2 nanofibers. *ScienceAsia* **51**, 2026001.
8. Orizu GE, Ugwuoke PE, Asogwa PU, Offiah SU (2023) A review on the inference of doping TiO_2 with metals/nonmetals to improve its photocatalytic activities. *IOP Conf Ser Earth Environ* **1178**, 012008.
9. Novianti N, Ramona F, Wellia DV, Muldarisnur M (2025) Enhanced light absorption of Cu and Ni doped TiO_2 nanostructures for photocatalytic water splitting applications. *J Fis Unand* **14**, 635–643.
10. Tarutani N, Kato R, Uchikoshi T, Ishigaki T (2021) Spontaneously formed gradient chemical compositional structures of niobium doped titanium dioxide nanoparticles enhance ultraviolet-and visible-light photocatalytic performance. *Sci Rep* **11**, 15236.
11. Somsongkul V, Chirawatkul P, Kongmark C (2021) Enhanced visible light response of TiO_2 nanoparticles by natural dyes. *ScienceAsia* **47S**, 69–75.
12. Rusinque B, Escobedo S, Lasa Hd (2021) Hydrogen production via Pd-TiO_2 photocatalytic water splitting under near-UV and visible light: Analysis of the reaction mechanism. *Catalysts* **11**, 405.
13. Sompech S, Jittabut P, Thaomola S, Audtarat S, Charee P, Dasri T (2021) Localized surface plasmon resonance for improving optical absorption in core-shell Ag@TiO_2 nanoparticles. *ScienceAsia* **47**, 340–346.
14. Qin L, Wang G, Tan Y (2018) Plasmonic Pt nanoparticles-TiO_2 hierarchical nano-architecture as a visible light photocatalyst for water splitting. *Sci Rep* **8**, 16198.
15. Moon HS, Yong K (2020) Noble-metal free photocatalytic hydrogen generation of CuPc/TiO_2 nanoparticles under visible-light irradiation. *Appl Surf Sci* **530**, 147215.
16. Birla PN, Arbuj S, Shinde MD, Joseph S, Rane S, Kulkarni S, Kale B (2023) Electroless Ni plated nanostructured TiO_2 as a photocatalyst for solar hydrogen production. *RSC Adv* **13**, 20068–20080.
17. Engge Y, Maulana F, Nurhuda M, Istiroyah I, Hakim L (2023) Enhancing hydrogen production through integration of electrolysis and photocatalysis in a cell. *Int J Energy Res* **2023**, 1–10.
18. Hinojosa-Reyes M, Camposeco-Solís R, Zanella R, González VR (2017) Hydrogen production by tailoring the brookite and Cu_2O ratio of sol-gel Cu-TiO_2 photocatalysts. *Chemosphere* **184**, 992–1002.
19. Lin Y, Jiang Z, Zhu C, Zhang R, Hu X, Zhang X, Zhu H, Lin SH (2017) The electronic structure, optical absorption and photocatalytic water splitting of (Fe + Ni)-codoped TiO_2: A DFT + U study. *Int J Hydrogen Energy* **42**, 4966–4976.
20. Jang D, Kim Y, Lee J, Shin H, Kang M (2024) Dual-functional Cu-Fe Co-doped TiO_2 photocatalyst for efficient hydrogen production and phenol degradation. *Surf Interfaces* **55**, 105394.
21. Kumar MK, Naresh G, Kumar VV, Vasista BS, Sasikumar B, Venugopal A (2021) Improved H_2 yields over Cu-Ni-TiO_2 under solar light irradiation: Behaviour of alloy nano particles on photocatalytic H_2O splitting. *Appl Catal B* **299**, 120654.
22. Anisha R, Vasam EKK (2022) Structural and optical properties of Ni-Cu doped TiO_2 synthesized by sol-gel method. *Asian J Chem* **34**, 3146–3150.
23. Pelaez M, Nolan NT, Pillai SC, Seery MK, Falaras P, Kontos AG, Dunlop PSM, Hamilton JWJ, et al (2012) A review on the visible light active titanium dioxide photocatalysts for environmental applications. *Appl Catal B* **125**, 331–349.
24. Kawawaki T, Kataoka Y, Ozaki S, Kawachi M, Hirata M, Negishi Y (2021) Creation of active water-splitting photocatalysts by controlling cocatalysts using atomically precise metal nanoclusters. *Chem Commun* **57**, 417–440.
25. Nie T, Li Z, Luo X, She Y, Liang L, Xu Q, Guo L (2022) Single bubble dynamics on a TiO_2 photoelectrode surface during photoelectrochemical water splitting. *Electrochim Acta* **436**, 141394.
26. Raguram T, Rajni KS (2019) Synthesis and analysing the structural, optical, morphological, photocatalytic and magnetic properties of TiO_2 and doped (Ni and Cu) TiO_2 nanoparticles by sol-gel technique. *Appl Phys A* **125**, 288.
27. Kumaravel V, Mathew S, Bartlett J, Pillai SC (2019) Photocatalytic hydrogen production using metal doped TiO_2: A review of recent advances. *Appl Catal B* **244**, 1021–1064.
28. Supardan SN, Sa'ari NS, Kamil SA, Rafaie HA, Fadzil AFM, Fauzi R, Mahmood MR, Noor NHM (2024) Effect of nickel doping concentration on the morphological and structural properties of titanium dioxide nanoparticles. *J Phys Conf Ser* **2680**, 012045.
29. Sun T, Liu E, Liang X, Hu X, Fan J (2015) Enhanced hydrogen evolution from water splitting using Fe-Ni codoped and Ag deposited anatase TiO_2 synthesized by solvothermal method. *Appl Surf Sci* **347**, 696–705.
30. Serafin J, Vendrell X, Dziejarski B, Amade R, Mestres L, Serrano I, Llorca J (2025) Synergistic enhancement of solar-driven hydrogen evolution via Ni-doped TiO_2–MXene hybrid photocatalyst. *Int J Hydrogen Energy* **179**, 151722.
31. Amin NAAM, Zaid HFM (2026) Optimizing TiO_2 photocatalysts with Co and Ni loading for improved photoelectrocatalytic hydrogen production. *Next Mater* **10**, 101417.
32. Kim S-B, Lee M-S, Lee S-Y, Park S-J (2026) Ni/Cu co-doping engineered TiO_2 for efficient solar-light-driven photocatalytic water treatment. *Surf Interfaces* **80**, 108292.
33. Thabet SM, Abdelhamid HN, Ibrahim SA, El-Bery HM (2024) Boosting photocatalytic water splitting of TiO_2 using metal (Ru, Co, or Ni) co-catalysts for hydrogen generation. *Sci Rep* **14**, 10115.
34. El-Bery HM, Naby MMA, Mohamed GG, El-Khouly ME, Zakaria MB (2024) Enhancing photocatalytic hydrogen generation on TiO_2 using thermally derived nickel-based cocatalysts from Hofmann-type cyanide coordination polymer flakes. *Int J Hydrogen Energy* **78**, 470–480.
35. Bilal ASS, Rodríguez-Ortiz G, Shahid M, Ballal S, Hassan H, Vashisht A, Banik N, Eshchanov T, et al (2025) Cu/Zr-doped TiO_2 nanocomposite based photocatalysts for sustainable visible-light hydrogen generation. *Results Chem* **17**, 102561.